



INSTITUT DE FRANCE  
Académie des sciences

# *Comptes Rendus*

---

## *Chimie*

Alan Gauffenic, Dominique Bazin, Christèle Combes, Michel Daudon and Hang-Korng Ea

### **Pathological calcifications in the human joint**


Volume 25, Special Issue S1 (2022), p. 517-534

Published online: 20 July 2022

<https://doi.org/10.5802/crchim.193>

**Part of Special Issue:** Microcrystalline pathologies: Clinical issues and nanochemistry

**Guest editors:** Dominique Bazin (Université Paris-Saclay, CNRS, ICP, France), Michel Daudon, Vincent Frochot, Emmanuel Letavernier and Jean-Philippe Haymann (Sorbonne Université, INSERM, AP-HP, Hôpital Tenon, France)

 This article is licensed under the  
CREATIVE COMMONS ATTRIBUTION 4.0 INTERNATIONAL LICENSE.  
<http://creativecommons.org/licenses/by/4.0/>



*Les Comptes Rendus. Chimie* sont membres du  
Centre Mersenne pour l'édition scientifique ouverte  
[www.centre-mersenne.org](http://www.centre-mersenne.org)  
e-ISSN : 1878-1543



Microcrystalline pathologies: Clinical issues and nanochemistry / *Pathologies microcristallines : questions cliniques et nanochimie*

# Pathological calcifications in the human joint

Alan Gauffenic<sup>ⓐ</sup>, Dominique Bazin<sup>ⓐ,\*,b,c</sup>, Christèle Combes<sup>ⓐ,d</sup>, Michel Daudon<sup>ⓐ,e,f</sup>  
and Hang-Korng Ea<sup>ⓐ</sup>

<sup>a</sup> Université de Paris, INSERM UMR 1132, BIOSCAR, Hôpital Lariboisière, Service de rhumatologie, DMU locomotion, APHP, Paris, France

<sup>b</sup> Université Paris-Saclay, CNRS, Institut de Chimie Physique, 91405 Orsay cedex, France

<sup>c</sup> Université Paris-Saclay, CNRS, Laboratoire de Physique des Solides, 91405, Orsay, France

<sup>d</sup> CIRIMAT, Université de Toulouse, CNRS, Toulouse INP – ENSIACET, 4 allée Emile Monso, 31030 Toulouse cedex 4, France

<sup>e</sup> INSERM, UMRS 1155, Sorbonne Université, Hôpital Tenon, 75020 Paris, France

<sup>f</sup> Service d'explorations fonctionnelles, Hôpital Tenon, AP-HP, 4, rue de la Chine, 75020 Paris Cedex 20, France

*E-mails:* alan.gauffenic@gmail.com (A. Gauffenic), dominique.bazin@universite-paris-saclay.fr (D. Bazin), christele.combes@ensiacet.fr (C. Combes), daudonmichel24@gmail.com (M. Daudon), korngea@yahoo.fr (H.-K. Ea)

**Abstract.** This contribution emphasizes the chemical complexity of abnormal cartilaginous deposits. First, we briefly describe some key techniques used to precisely describe their physicochemical characteristics. Then, we present the main chemical and structural characteristics of these two chemical phases, of either biological or synthetic origins. Finally, we discuss selected examples of calcification characterization.

**Keywords.** Cartilage, Human joint, Pathological calcifications, Scanning electron microscopy, Synchrotron radiation.

*Published online:* 20 July 2022

## 1. Introduction

Various epidemiological studies [1,2] rank osteoarthritis (OA), a rheumatic musculoskeletal disorder, as the most common joint disorder in the world. Thus the economic burden of OA on patients as well as on society is considerable. OA not only causes

pain, but loss of function and consequent disability in adults. The American Joint Replacement Registry (AJRR) and the American Academy of Orthopedic Surgeons (AAOS), reported 1.2 million patients with over 1.7 million hip and knee replacement procedures in America in May 2020 [3,4].

OA affects the entire joint [5]. More precisely, the pathological modifications seen in OA encompass degradation of the articular cartilage, thicken-

\* Corresponding author.

ing of the subchondral bone, osteophyte formation, variable degrees of synovial inflammation, degeneration of ligaments and menisci in the knee, and hypertrophy of the joint capsule [6].

Regarding cartilage, some investigators consider articular calcium phosphate crystals as “innocent bystanders” or the natural consequence of the joint damage [7]. Recent studies present evidence that intra-articular calcium phosphate crystals can elicit synovial inflammation and cartilage degradation, suggesting that these crystals play a direct pathogenic role in OA [8,9]. As stated by Murphy *et al.* [10] even if the presence of intra-articular calcium phosphate crystals is a consequence of joint damage, these crystals participate actively in aggravating the symptoms and signs of OA, especially via their effects on the synovium. Finally, Liu *et al.* [11] have extracted crystals from human osteoarthritic knee cartilage: they noticed that such crystals induce the production of proinflammatory and catabolic mediators (NO, MMP-13 and PGE2) in human primary chondrocytes and synoviocytes.

Cartilage calcifications can comprise different crystalline calcium phosphate phases: a calcium orthophosphate phase, i.e. carbonated apatite (CA), and two calcium pyrophosphate (CPP) phases, particularly monoclinic, and triclinic, CPP dihydrate phases (m-CPPD) and (t-CPPD) [12,13]. Carbonated apatite (CA) crystals are observed in 90%–100% of OA cartilage and associated with m- or t-CPPD crystals in 20%. The inflammatory mechanisms triggered by these different calcium phosphate crystal types are similar. However, m-CPPD has been reported to induce a more potent pro-inflammatory response via NF- $\kappa$ B pathway activation leading to the production of interleukin (IL)1 $\beta$ , IL6 and IL8 [14].

In this contribution, we present some recent investigations focused on the relationship between OA and calcifications. Accordingly we will present some selected physicochemical results based either on in-lab techniques or those available on large scale synchrotron radiation facilities, and discuss the advantages and limitations of these techniques. We will start with some general considerations on the relationship between disease and calcification, and a short review of the different techniques which have already been used to characterize pathological calcifications. Then some physico-chemical characteristics of calcium phosphate phases (CA and CPPD) in-

involved in joint calcifications will be presented, and finally the detailed elemental, structural and morphological characterization of calcified cartilage will be described.

## 2. Brief summary of analytical methods for characterization of physiological and pathological calcifications

Following the example of Yavorsky *et al.* [15], we consider several different families of techniques which can be classified as either imaging or spectroscopic.

### 2.1. Imaging techniques

Firstly, ultrasonography (US) [16], conventional radiography (CR) [16] and computed tomography (CT) [17,18], are routine imaging techniques typically available in hospitals. Recently, Cipolletta *et al.* [19] have evaluated and compared the accuracy of conventional radiography and musculoskeletal ultrasonography in the diagnosis of calcium pyrophosphate crystal deposition disease showing that these two techniques are complementary and aid diagnosis. US appeared helpful, and more sensitive than CR, in revealing CPPD-based calcification.

In clinical routine, polarized light microscopy is useful for identifying CPP crystals, and discriminates them from crystalline monosodium urate (MSU), but is insufficient for CA crystals which are too small. The spatial resolution of these three imaging techniques is currently sufficient for medical diagnosis but not particularly applicable in clinical research.

MicroCT, and contrast-enhanced CTs (CE-CT), can provide images of cartilage samples and calcifications but application at the *in vivo* scale (under 6 micrometers resolution) appears challenging. Dual-energy computed tomography (DECT) has recently emerged as a promising tool for chemical discrimination of cartilage calcifications. Pascart *et al.* [20] published a first proof of concept study on the potential of DECT for differentiating CPPD from apatite on subchondral and trabecular bone. Subsequently, the DECT approach has been used to effectively distinguish calcium orthophosphate (such as CA) and CPP crystal deposition in human joints *in vivo*. DECT can differentiate intra-articular CPP deposits from bone apatite [21].

Multi-energy spectral photon-counting CT (SPCCT) is a novel imaging technique which has potential advantages over DECT in characterizing MSU crystal deposits but needs to be further evaluated in the assessment of calcification pathologies *in vivo* [22,23].

Among conventional techniques, only ultrasonography is able to detect calcium phosphate crystal deposition, while advanced techniques, micro-CT and SPCCT, are both able to detect the crystals at micrometre spatial resolution ( $0.018 \times 0.018 \times 0.018 \text{ mm}^3$  and  $0.090 \times 0.090 \times 0.090 \text{ mm}^3$  respectively). However, only SPCCT has been reported to be able to discriminate between CPPD and HA crystal deposits [24].

Field emission scanning electron microscopy (FE-SEM) plays a key role in OA research and achieves submicrometre spatial resolution [25,26]. Since the emergence of such technology (which replaces a single tungsten filament with a sharp pointed tip as the electron source), observations of calcifications on the surface of cartilage can be performed at low voltage (between 0.5 and 2 kV) without the need for conventional sample preparation such as surface deposition of carbon. As Figure 1 shows, micrometre scale FE-SEM images can distinguish between CA and CPPD crystals by their morphology [12].

In pathological calcifications, CA deposits generally manifest as spherical structures constituted of nanocrystal agglomerates [9,27,28], while CPPD crystals are larger and display an acicular morphology [29], as can be seen in Figure 1. More generally, the well understood relationship between crystal morphology, crystal symmetry, and chemical identity, constitutes a solid basis of crystallo-chemical analysis [30,31]. The spherical morphology of CA results from an agglomeration of nanocrystals of dimensions typically less than one hundred nanometres [32] and with a platelet morphology [33,34].

On an FE-SEM apparatus, an X-ray detector is usually positioned to gather information on the elemental composition of the calcification through X-ray fluorescence induced by the primary electrons [25,26]. This can give the Ca/P atomic ratio, which may be informative regarding the nature of the calcium orthophosphate phase (especially for dicalcium phosphate dihydrate (DCPD: Ca/P = 1) or octacalcium phosphate (OCP: Ca/P = 1.33), which are

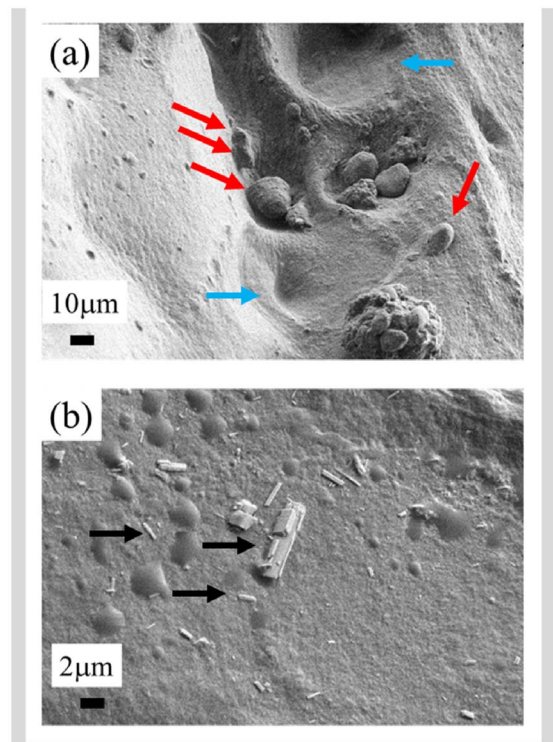


**Figure 1.** Examples of cartilage calcifications: (a) Agglomerates of several apatite crystallites (red arrows) localized in structures suggestive of chondrons (blue arrows). (b) Typical rod-shaped m- or t-calcium pyrophosphate dihydrate crystals (black arrows).

known as CA precursor phases) [35] except for biological CA which is a non-stoichiometric apatite with a Ca/P ratio lower than 1.67 (stoichiometric hydroxyapatite (HA)) [36,37] and which can reach Ca/P values as low as that of OCP.

Nanometer scale imaging informs the clinician about the very first steps of pathogenic calcification [38]. There is a wide diversity of pathological calcification nucleation mechanisms, which may be homogeneous [39] or heterogeneous [40]. In the latter case, the role of vesicles [41,42], DNA [43], or proteins like elastin [44,45], as pathological calcification nuclei have been discussed. At this point, we emphasize that to determine the chemical nature of intravascular calcifications, and more general nanometer scale deposits, various techniques such as electron energy loss micro-spectroscopy [42,46] are available. Several papers discuss the presence of vesicles in car-

tilage [47–49]. For instance Anderson [47] has identified vesicles of very different size ( $\sim 300 \text{ \AA}$ – $1 \text{ }\mu\text{m}$ ) within the cartilage matrix of the upper tibial epiphyseal plate of normal mice.

Finally, it is worth noting that 3D images can be obtained through classical tomography [50,51] in a typical hospital environment with a spatial resolution around  $100 \text{ }\mu\text{m}$  [52]. Using synchrotron radiation as a probe, Marenzana *et al.* [53] demonstrate that it is moreover possible to collect microCT data with an effective resolution of approximately  $9 \text{ }\mu\text{m}$ .

## 2.2. Vibrational spectroscopies

As emphasized previously, the various calcium phosphate phases in OA calcified cartilage (CA, m-CPPD and t-CPPD) require physico-chemical techniques, more specifically vibrational spectroscopies such as Raman [54–56] or Fourier transform infra-red (FT-IR) [57–61], which are advantageously non-destructive and label-free, for chemical analysis of biological tissues [54–61]. They detect vibrational energy levels and phonons of materials, and comparison with data bank reference spectra yields precise chemical and structural information [62]. These two spectroscopies are complementary, and both techniques are usually required to comprehensively measure the vibrational modes of a solid or dissolved molecule. In the case of pathological calcifications, advantages and limitations of these two spectroscopies with respect to sample preparation and data acquisition have been discussed by Daudon *et al.* [58]. At this point, let's recall that a Raman spectrum depicts the optical transitions between the various rotational–vibrational energy states of molecules, or ionic groupments and therefore enables precise characterization of material chemical composition [54–56,63,64]. The “Raman active” energy transitions observed in Raman spectra originate from a change in the polarizability of a molecular entity, i.e. the distortion of its electron cloud upon interaction with the incident light (i.e. a strong oscillating electromagnetic field in the UV, visible, or infrared energy domain) [56]. Raman spectroscopy has been applied to several kinds of biological samples encompassing fluids [65], cells [66], minerals as physiological [67] and pathological calcifications [68] and tissues [69].

Regarding FT-IR spectroscopy, or mid-FTIR region spectroscopy (wavenumber between  $400$ – $4000 \text{ cm}^{-1}$ ), the classical FTIR microscope experimental set-up which utilizes conventional sources (global) can collect chemical images with a spatial resolution of approximately  $5$ – $10 \text{ }\mu\text{m}$  depending on wavelength [70]. This spatial resolution can be significantly improved by combining atomic force microscopy and IR lasers [71–76], in which case spatial resolution is determined by the tip dimension and thus not diffraction limit constrained, and can be around  $10 \text{ nm}$ . Note that Optical PhotoThermal IR spectroscopy represents another opportunity, based on a pump–probe architecture using two laser sources, one for mid-infrared excitation (the pump) and the other for measuring the photothermal effect (the probe). With this geometry, it is possible to acquire IR spectra with a lateral resolution around  $500 \text{ nm}$  [75,77–84].

Numerous investigations (see review [85]) have been performed on cartilage following the pioneering work of Camacho *et al.* [86] and Potter *et al.* [87]. In terms of the preparation protocol, Spencer *et al.* [88] have clearly shown that the spectrum of fresh cartilage displays an altered amide I ( $1590$ – $1720 \text{ cm}^{-1}$ )/amide II ( $1480$ – $1590 \text{ cm}^{-1}$ ) peak ratio after 24 h, which corresponds to a significant alteration of the cartilage tissue, the amide I being correlated with the amount of collagen. In the case of CA, the  $\nu_1$  and  $\nu_3 \text{ PO}_4$  stretching vibration modes occur at  $960$ – $962 \text{ cm}^{-1}$  and  $1035$ – $1045 \text{ cm}^{-1}$  respectively, while the  $\nu_4 \text{ PO}_4$  bending mode corresponds to the bands at  $602$ – $563 \text{ cm}^{-1}$ . Finally, note the absence of the bands at  $3570$  and  $633 \text{ cm}^{-1}$ , which correspond to the stretching and vibrational modes of the  $\text{OH}^-$  groups characteristic of hydroxyapatite [62]. We will show that other techniques such as X-ray absorption spectroscopy when applied to nanometer scale materials [89–91] may also give essential information regarding pathological cartilage calcifications [92–96].

## 3. Some physicochemical aspects of the calcium phosphate phases in pathological joint calcifications

Two distinct calcium phosphate crystalline families are prominent in synovial fluids and cartilage, namely calcium pyrophosphate dihydrates and calcium orthophosphate [97]. In terms of the former,

both t-CPPD and m-CPPD phases occur in joint calcifications. Among the latter family, CA is the main phase encountered; it corresponds to a non-stoichiometric nanocrystalline carbonated apatite family (CA:  $\text{Ca}_{10-x}(\text{PO}_4)_{6-x}(\text{HPO}_4, \text{CO}_3)_x(\text{OH})_{2-x}$ ) [98,99]. Other crystalline calcium phosphate phases have been occasionally identified in synovial fluids and cartilage: octacalcium phosphate (OCP;  $\text{Ca}_8(\text{HPO}_4)_2(\text{PO}_4)_4 \cdot 5\text{H}_2\text{O}$ ), tricalcium phosphate ( $\text{Ca}_3(\text{PO}_4)_2$ ) [100], dicalcium phosphate dihydrate (DCPD) [101], and whitlockite ( $\text{Ca}_9\text{Mg}(\text{HPO}_4)(\text{PO}_4)_6$ ) [60,102], based essentially on crystal morphology and size, and elemental composition [103]. As pointed out by Yavorsky *et al.* [14], such diversity of calcium phosphate phases calls for physicochemical characterization techniques, and even a combination of several techniques, in addition to standard staining procedures which may help to detect pathological calcifications [27,28,104] but are not able to distinguish among these different calcium phosphate phases. Later we present some physicochemical aspects relevant to the main calcium phosphates identified in OA cartilage calcifications: CA and m-/t-CPPD phases.

### 3.1. Biological and synthetic nanocrystalline carbonated apatites

There are several excellent publications and reviews on the structural characteristics of phosphocalcic apatites [105–107]. Stoichiometric hydroxyapatite (HA:  $\text{Ca}_{10}(\text{PO}_4)_6(\text{OH})_2$ ) which crystallizes in the monoclinic P<sub>2</sub><sub>1</sub>/b group (Figure 2) has generally been used as a model for biological apatites (bone mineral and tooth enamel). Unlike stoichiometric HA, biological apatites crystallize in the hexagonal P<sub>6</sub><sub>3</sub>/m space group with the following unit cell parameters  $a = b = 9.41844 \text{ \AA}$  and  $c = 6.88374 \text{ \AA}$  [105,106].

The presence of significant amounts of carbonate ions located in the  $\text{PO}_4^{3-}$  sites (type B carbonated apatite) and the  $\text{OH}^-$  sites (type A carbonated apatite) in apatites from pathological calcifications or normal hard tissues constitutes one of the main differences from the HA stoichiometric model [108]. Long a topic of debate, non-stoichiometric carbonated apatite is widely accepted as a model for biological hard tissue apatites, and described by the general chemical formula:  $\text{Ca}_{10-x}\square_x(\text{PO}_4)_{6-x}(\text{CO}_3)_x(\text{OH})_{2-x}\square_x$  with  $0 \leq x \leq 2$  ( $\square$  is a vacancy) [109–111]. The

presence of hydrogen phosphate ( $\text{HPO}_4^{2-}$ ) ions in  $\text{PO}_4^{3-}$  sites has also been reported in biological apatites [112,113]. Both divalent ions (carbonate and hydrogen phosphate) substituting for  $\text{PO}_4^{3-}$  are associated with a charge compensation mechanism involving the formation of one vacancy on a cationic site and one on a monovalent anionic site. Each divalent ion replacing  $\text{PO}_4^{3-}$  is thus associated with a missing  $\text{OH}^-$ , which explains why bone apatite is depleted in hydroxide ions.

In addition to large substitution capacity, tolerance of defects (mainly calcium and hydroxyl deficient non-stoichiometric apatites), nanocrystalline apatites present specific physicochemical and structural characteristics including exceptional surface reactivity, making this compound adaptable to various biological conditions and functions [114,115]. This reactivity is related to the existence on the nanocrystal surface of an hydrated layer containing mainly loosely bound divalent ions which can be easily exchanged in solution with cations, anions or proteins [116]. The carbonate content may be a clinical marker of alkaline medium. Thus, it is high in CA crystals identified in OA and bone. By contrast, it is low in kidney stones, except in the case of urinary tract infection by urease-splitting bacteria [117,118].

The hydrated surface layer responsible for the strong surface reactivity of nanocrystalline apatites (ageing/maturation, ionic exchange, adsorption) is the most interesting structural feature but also the most complex to characterize. The latter can often be achieved with a combination of methods including chemical titrations and spectroscopic techniques such as vibrational spectroscopies (FTIR and Raman) and solid state nuclear magnetic resonance (NMR) [119,120]. The model of apatite nanocrystals based on an apatitic core and a more or less structured surface hydrated layer including non-apatitic domains is accepted but the precise description of the organization within this hydrated layer is still discussed. The reader will find illustrations of the apatite nanocrystal model in several papers [111,116].

Biomimetic nanocrystalline carbonated apatites can be synthesized by double decomposition between a soluble calcium salt solution and a soluble phosphate salt solution with a large excess of phosphate and carbonate ensuring pH buffering around physiological pH [116]. Precipitation of apatite is achieved by rapidly pouring the calcium solution into

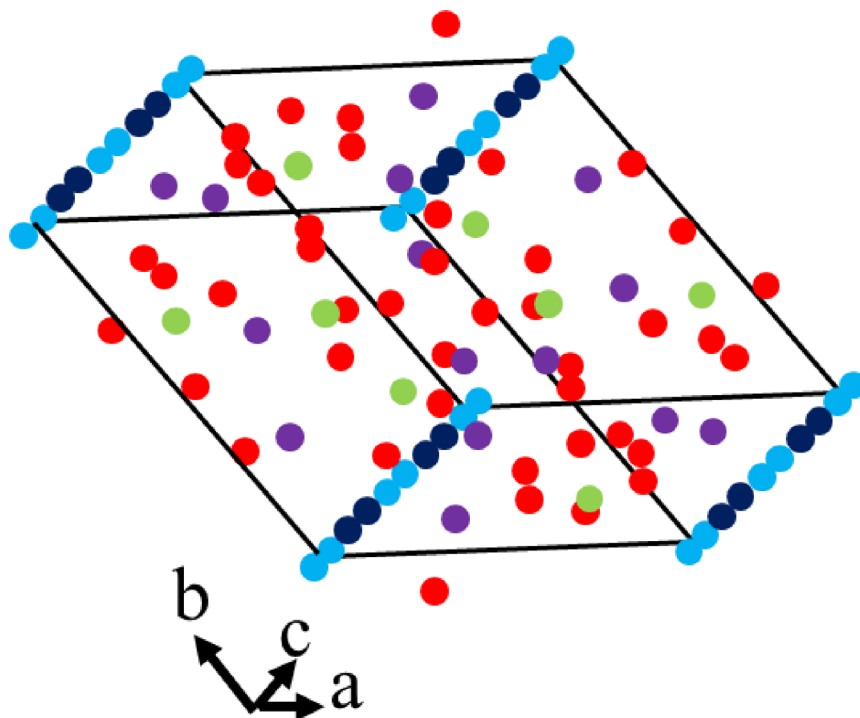


**Figure 2.** Spatial repartition of the different atoms in the case of stoichiometric hydroxyapatite (HA:  $\text{Ca}_{10}(\text{PO}_4)_6(\text{OH})_2$ ). Hydrogen and oxygen atoms of the hydroxyl groups represented in blue and dark blue respectively are located on the  $c$ -axis.

the phosphate/carbonate solution at room temperature and ageing the precipitate in the mother solution for variable periods of time. It is then filtered, washed, freeze-dried, and kept dry in a freezer to prevent from any transformations. This method yields plate-like apatite nanocrystals with a size and morphology analogous to bone apatite crystals (Figure 3).

Biological and synthetic apatite nanocrystals show a thin platelet morphology elongated toward the  $c$  axis with crystal dimensions of less than 100 nm, and even 50 nm, in length and a few nanometers in thickness [121]. TEM and SEM images of biological and synthetic nanocrystalline carbonated apatites are presented in Figure 3.

Finally, it is worth pointing out the presence of essential biological trace elements namely Mg, Fe, Sr, Se and Zn. In the cartilage examples we will show that the Zn content may be related to inflammation (Section 3.2) [122–124].

### 3.2. *Biological and synthetic calcium pyrophosphate phases*

As opposed to calcium orthophosphates, and especially apatites which have been extensively studied over many decades, the physicochemistry of calcium pyrophosphate phases of biological interest are not well documented although they were identified more than 60 years ago in menisci and synovial fluids [125, 126]. One of the main reasons is certainly related to the difficulty of obtaining pure synthetic CPPD compounds in large enough amounts to be able to thoroughly study the formation of those phases involved in biological processes and their detailed characterization.

Calcium pyrophosphate hydrated phases ( $\text{Ca}_2\text{P}_2\text{O}_7 \cdot n\text{H}_2\text{O}$ ) have been studied in several excellent investigations [127–131]. Several forms of pure crystalline and amorphous calcium pyrophosphate hydrates have also been synthesized [131] including the two phases detected in joints of OA patients, m-CPPD and t-CPPD both of chemical



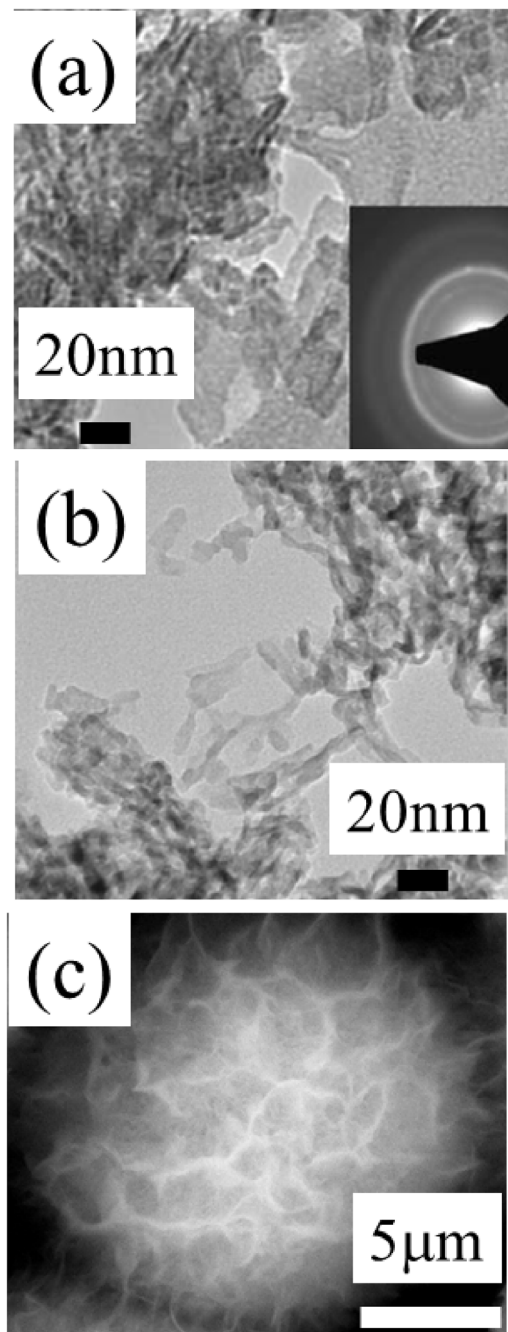


**Figure 3.** (a) TEM observation of bone tissue cross-section. (b) TEM observation of synthetic carbonated apatite (from Ref. [121]). (c) SEM observation of a pathological calcification composed of apatite (kidney stone).

formula  $\text{Ca}_2\text{P}_2\text{O}_7 \cdot 2\text{H}_2\text{O}$ . The existence of four other forms, namely one calcium pyrophosphate monohydrate phase ( $\text{Ca}_2\text{P}_2\text{O}_7 \cdot \text{H}_2\text{O}$ ) [132], two monoclinic calcium pyrophosphate tetrahydrates (CPPT:  $\text{Ca}_2\text{P}_2\text{O}_7 \cdot 4\text{H}_2\text{O}$ ) denoted m-CPPT- $\alpha$  and m-CPPT- $\beta$ , and an amorphous phase, denoted a-CPP ( $\text{Ca}_2\text{P}_2\text{O}_7 \cdot n\text{H}_2\text{O}$  with  $n$  around 4) [131,133–135] must also be mentioned. m-CPPT  $\beta$  and a-CPP phases are *in vitro* precursor phases of m/t-CPPD phases [126,136]. In acidic medium t-CPPD is the thermodynamically most stable crystalline phase of the CPP hydrates, followed by m-CPPD and then m-CPPT  $\beta$  phases.

Hydrolysis of some pyrophosphate ions ( $\text{P}_2\text{O}_7^{4-}$ ) into orthophosphates ( $\text{HPO}_4^{2-}$ ) can occur in the solid or in solution according to (1); this reaction is favored by acidic pH and/or increase of temperature in solution, and also at high temperature as a solid state reaction (internal hydrolysis) [130,137]. The presence of orthophosphate ions may stabilize some CPP hydrated phases and/or explain the co-existence of calcium orthophosphate (CA) and calcium pyrophosphate (m-CPPD and/or t-CPPD) phases in joint calcifications.



A one-step fast protocol allowed the synthesis of the four CPP hydrated phases of biological interest (m-CPPD, t-CPPD, m-CPPT  $\beta$  and a-CPP) by controlling the pH and temperature during their precipitation by a double decomposition reaction between potassium pyrophosphate and calcium nitrate salt solutions [131]. With this method, we obtained pure m-CPPD powder and fully solved the m-CPPD structure including precise determination of hydrogen atom positions using Rietveld refinement of complementary data from synchrotron powder X-ray, and neutron, diffraction (Figure 4) [135]. Its unit-cell corresponds to the monoclinic system  $\text{P}2_1/n$  and its parameters are:  $a = 12.60842(4) \text{ \AA}$ ,  $b = 9.24278(4) \text{ \AA}$ ,  $c = 6.74885(2) \text{ \AA}$  and  $\beta = 104.9916(3)^\circ$ . The m-CPPD cell includes four formula units. The volume per formula unit is  $189.93(1) \text{ \AA}^3$ ; it is almost equal to that of the t-CPPD structure,  $189.32(9) \text{ \AA}^3$ , the other CPPD phase found in OA joints, which presents a high inflammatory potential but lower than that of m-CPPD [138,139]. These new structural data on this pathological phase, with the highest inflammatory potential among the crystalline CPPD forms [140]



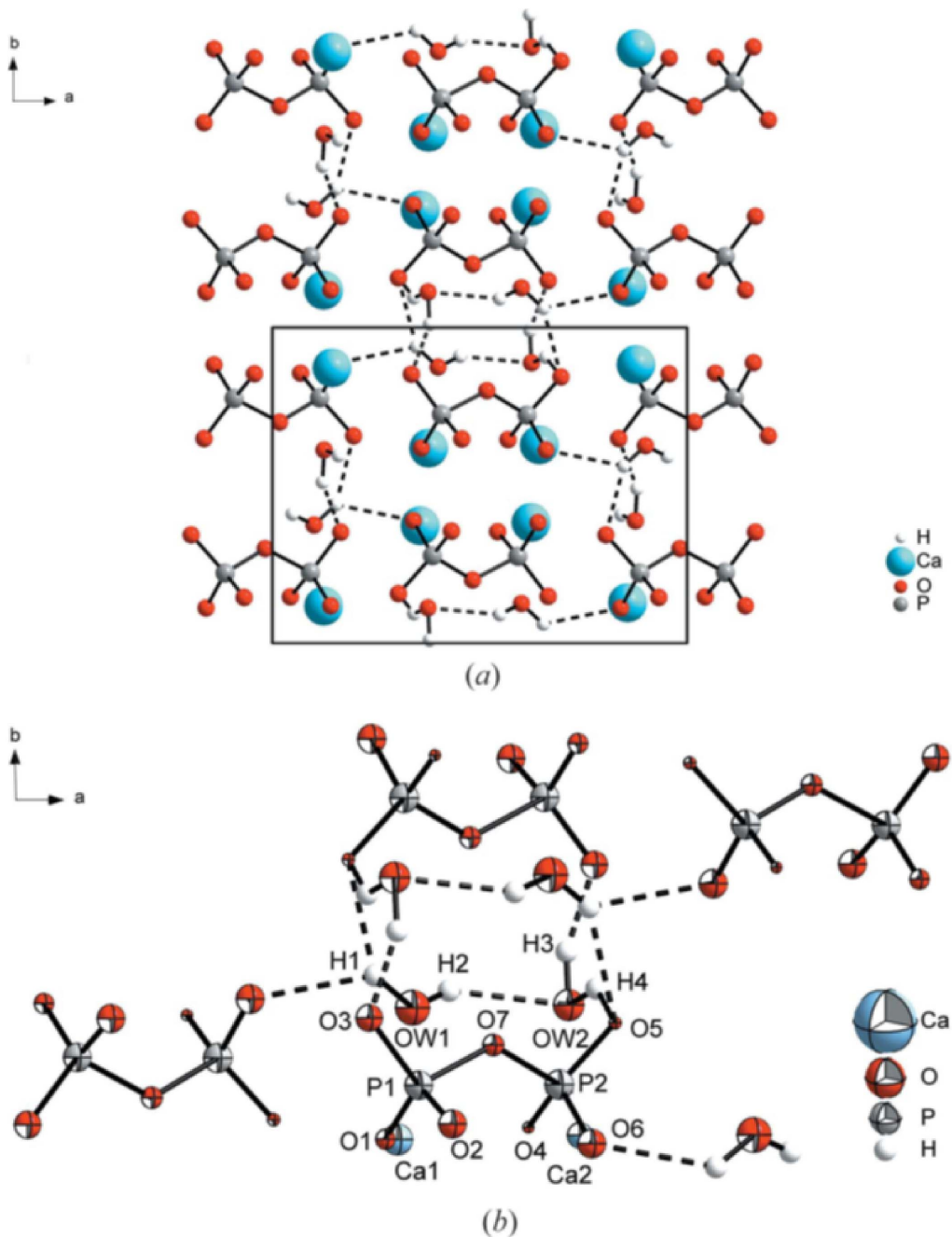


**Figure 4.** (a) Crystal structure of the m-CPPD phase and (b) representation of m-CPPD crystal structure showing the hydrogen bond network. Displacement ellipsoids are drawn at the 50% probability level. (Reprinted from Ref. [135].)

are of particular importance to further understand *in vivo* phenomena related to crystal structure-inflammatory response relationships in OA.

Detailed structural aspects of the biogenic CPPD phases have also been investigated by  $^1\text{H}$ ,  $^{31}\text{P}$  and  $^{43}\text{Ca}$  MAS solid state NMR spectroscopy leading to

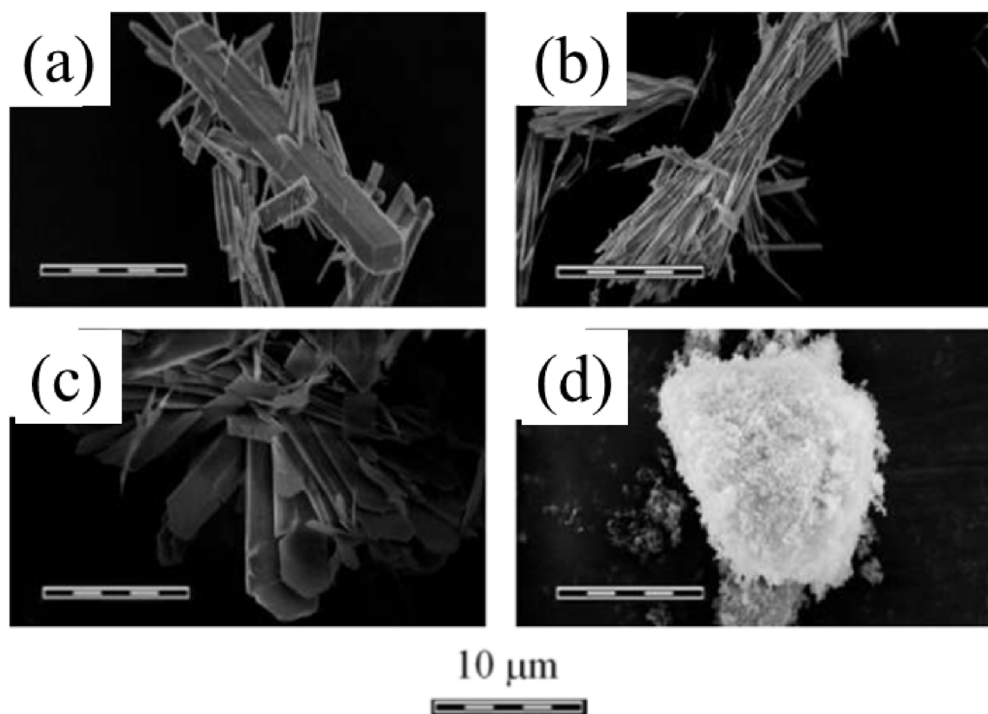


**Figure 5.** Morphologies of the different synthetic crystalline and amorphous phases of the calcium pyrophosphate hydrates of biological interest: (a) t-CPPD, (b) m-CPPD, (c) m-CPPT  $\beta$  and (d) *a*-CPP. (Reprinted from Ref. [131].)

informative fingerprints characterizing each phase [129]. Vibrational spectroscopies (FTIR and Raman) allow the different CPPD phases to be identified and provide valuable information on the conformations of the  $P_2O_7^{4-}$  ions [131]. Indeed the flexibility of the pyrophosphate anion in the structure leads to different P–O–P bridge vibrations, and variation of the P–O–P angle, resulting in an effective means of clearly identifying the four calcium pyrophosphate hydrated phases (m-CPPD, t-CPPD, m-CPPT  $\beta$  and *a*-CPP). Gras *et al.* [131] have published a full description of the characteristic Raman and FTIR spectroscopy bands using reference synthetic phases.

The four main synthetic crystalline and amorphous phases of calcium pyrophosphate hydrates display very different morphologies (Figure 5) [131, 139]. The two CPPD polymorphs showed different acicular crystal habits: thin needles for m-CPPD (Figure 5b) and rods for t-CPPD (Figure 5a). Figure 5a shows t-CPPD synthetic crystal morphology, which appears analogous to that of biological crystals ob-

served at the surface of calcified cartilage (Figure 1b). m-CPPT  $\beta$  (Figure 5c) has a faceted plate morphology related to the layered structure of this compound [126] and *a*-CPP appears as agglomerates of round nanoparticles of about 100 nm (Figure 5d). In addition to the different morphology of these four hydrated CPP phases, the distribution of pyrophosphate groups on the surface planes could explain the difference in inflammatory potential reported during *in vitro* and *in vivo* tests [139,140].

McCarty *et al.* [126] have proposed a scheme which establishes some structural evolution between all the calcium pyrophosphate forms.

#### 4. Selected results on characterization of cartilage calcifications

##### 4.1. X-ray absorption spectroscopy

Nguyen *et al.* [92] have characterized the chemical composition of medial and lateral cartilage from femoral condyles and tibial plateau (Figure 6) by

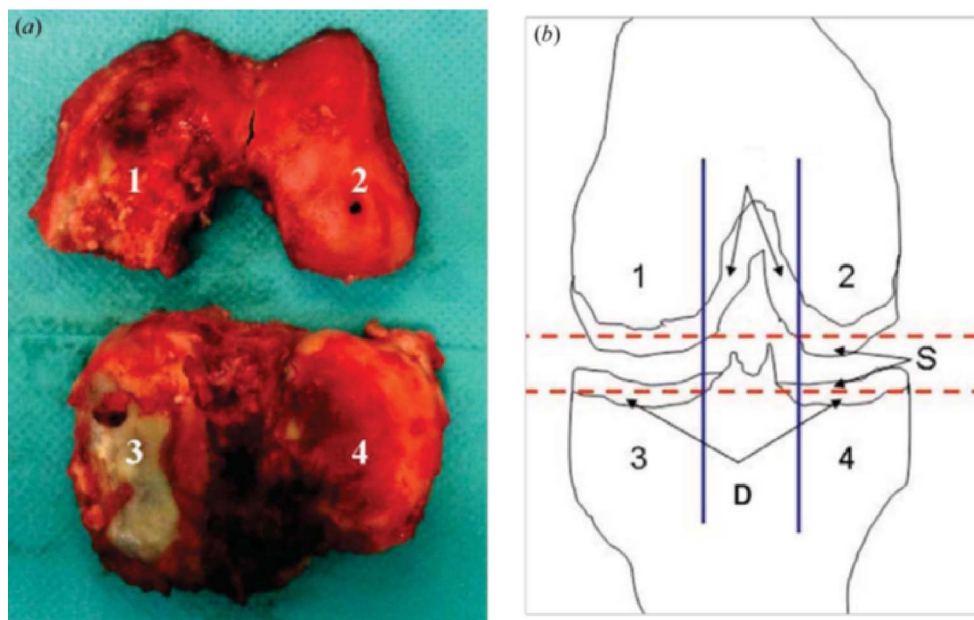


**Figure 6.** Knee joint specimen obtained during arthroplasty (a), and a schematic of the sample collection protocol (b). The specimen included femoral condyle and tibial plateau cartilage from both the medial and the lateral compartments (a). Cartilage areas are labelled as follows: 1—medial condyle; 2—lateral condyle; 3—medial tibial plateau; 4—lateral tibial plateau; S—superficial layer; D—deep layer (b) (from Ref. [92]).

FT-IR spectroscopy (Figure 7), and X-ray absorption spectroscopy (XAS) at the Ca K-absorption edge. The different regions of interest investigated are shown in Figure 6.

Figure 7 shows FTIR absorption spectra of cartilage samples. The absorption bands of carbonated apatite (CA) and calcium pyrophosphate dihydrate (CPPD) are well documented. Regarding CA, the  $\nu_1$  and  $\nu_3$  P–O stretching vibration modes occur at  $960\text{--}962\text{ cm}^{-1}$  and  $1035\text{--}1045\text{ cm}^{-1}$ , respectively, while the  $\nu_4$  O–P–O bending mode corresponds to the doublet at  $602\text{--}563\text{ cm}^{-1}$ . The bands at  $3570$  and  $633\text{ cm}^{-1}$ , corresponding to the stretching and vibrational modes of the  $\text{OH}^-$  groups characteristic of hydroxyapatite, are absent from CA. Regarding m-CPPD, O–P–O bending is observed at  $535\text{ cm}^{-1}$  and  $508\text{ cm}^{-1}$ . P–O stretching vibrations correspond to absorption bands at  $923\text{ cm}^{-1}$  and  $991\text{ cm}^{-1}$ , whereas asymmetric stretching vibrations give rise to absorption bands at  $1037\text{ cm}^{-1}$  and  $1089\text{ cm}^{-1}$ .

Synchrotron generated XAS is a sensitive technique which has been used to characterize the local environment of specific elements [137,141] such

as S [95], Ca [92,142–145], Zn [94,146,147], Se [96], Pb [93], and Sr [148,149], in pathological calcifications. While for FTIR spectroscopy samples must be ground in a mortar to reduce the average particle size to 1 or 2  $\mu\text{m}$ , XAS experiments can be performed directly on the biological sample with minimal preparation [92,142]. Note that many medically important substances such as anticancer molecules [150,151] and nanometer scale materials [152,153] can also be characterized with XAS spectroscopy [154–156].

Eichert *et al.* [157] demonstrate that XAS at the Ca K edge distinguishes between different non-apatitic calcium phosphates, namely dicalcium phosphate dihydrate, anhydrous dicalcium phosphate, octacalcium phosphate, amorphous calcium phosphate, beta tri-calcium phosphate and alpha tri-calcium phosphate (Figure 8).

The XAS spectra have been rationalized by Eichert *et al.* [157]. With increasing energy, we encounter the most intense resonance, known as the “white line”, corresponding to the main  $1s \rightarrow np$  transition (Figure 9), exhibiting a characteristic three peak

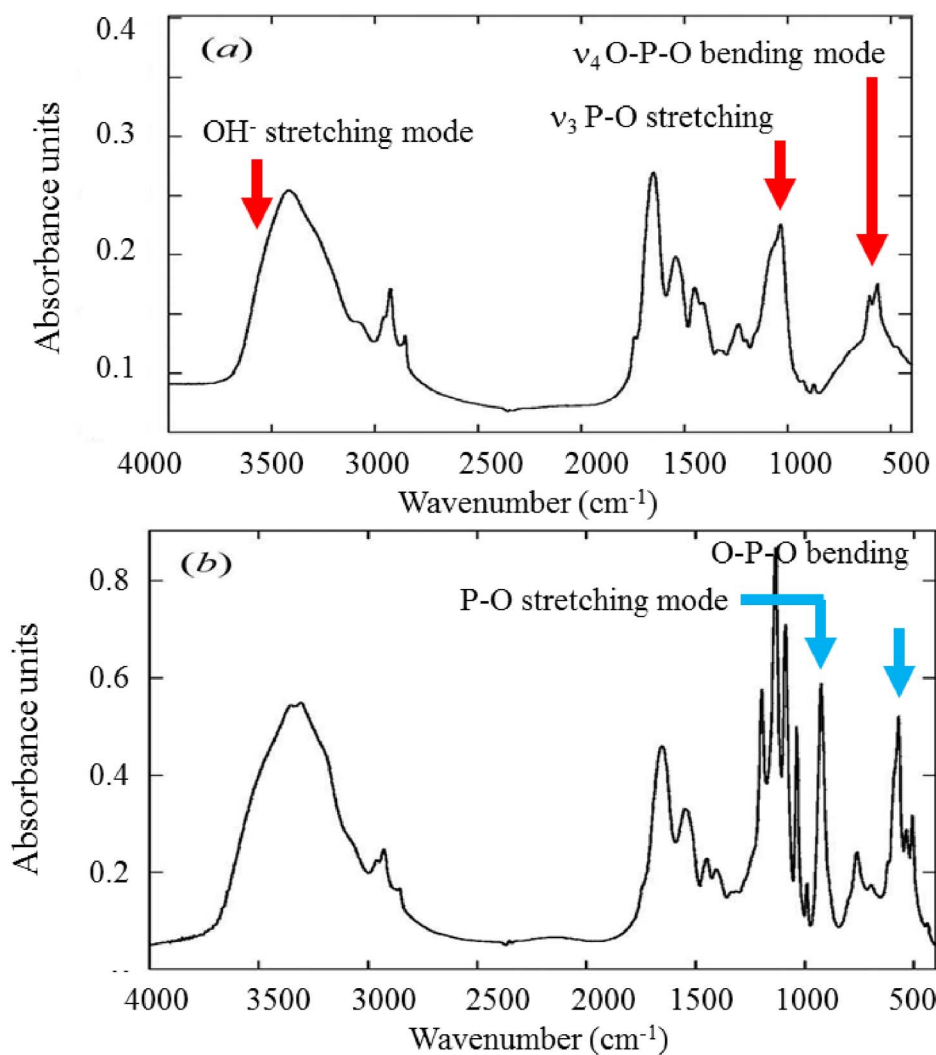


**Figure 7.** FT-IR absorption spectra of cartilage samples exhibiting pathological calcifications, namely, CA (a) and m-CPPD (b) (from Ref. [75]). Regarding m-CPPD, other IR bands are visible such as those related to  $\nu\text{PO}_3$  ( $990\text{--}1200\text{ cm}^{-1}$ ) and  $\nu\text{OH}$  ( $3100\text{--}3600\text{ cm}^{-1}$ ) (see Ref. [131]).

structure: a shoulder (labelled B, 4047 eV) on the low energy side that remains unaltered across the series, assigned to the  $1s \rightarrow 4s$  transition, a principal peak (C) corresponding to the allowed  $1s \rightarrow 4p$  transition comprising two components (C1 and C2), whose relative intensities depend on Ca type (I or II) and may reflect deviation from stoichiometry in the samples [158]. D peak (4058.6 eV) corresponds to transitions to unoccupied states, mainly 5s states [159]. In addition, more XANES structures (labelled from E to H), mainly

due to multiple scattering contributions, are resolved at higher energies for all compounds.

Nguyen *et al.* [92] investigated 12 cartilage samples by FTIR and X-ray absorption spectroscopy. FTIR spectroscopy detected CA and CPPD crystals in four, and three, out of 12 samples respectively. Three reference compounds were used, biological m-CPPD, CA, and amorphous carbonated calcium phosphate (ACCP).

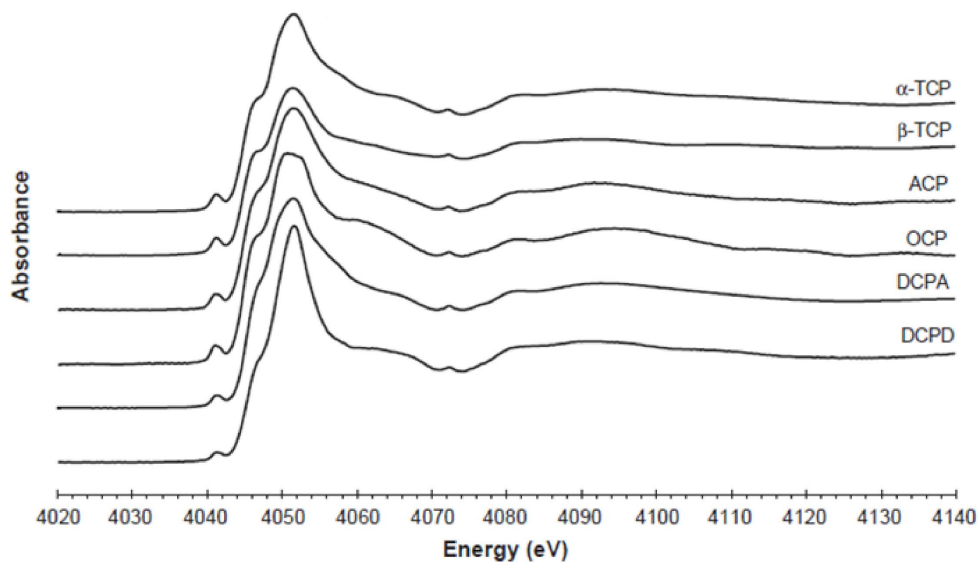


**Figure 8.** XANES spectra at the Ca K-edge of different non-apatitic calcium phosphate compounds. (DCPD: dicalcium phosphate dihydrate, DCPA: anhydrous dicalcium phosphate, OCP: octacalcium phosphate, ACP: amorphous calcium phosphate,  $\beta$ -TCP: beta tri-calcium phosphate,  $\alpha$ -TCP: alpha tri-calcium phosphate). Reprinted from Ref. [157].

A striking result arises from the fact that calcium XAS spectra differ between calcified and non-calcified cartilage areas. In calcified areas calcium appears to be mainly associated with crystalline phase(s). In a more recent investigation, Nguyen *et al.* [12] demonstrate that mineralization involved several compartments, and processes associated with an increase in the expression of genes regulating inorganic phosphate and pyrophosphate homeostasis, which suggests a switch toward a promineralizing chondrocyte phenotype in OA.

#### 4.2. Heavy elements in cartilage

Techniques specific to synchrotron radiation such as  $\mu$ X-ray fluorescence or  $\mu$ XAS can also be used to detect heavy elements in cartilage. Jarup [160], for example, has pointed out that the main threats to human health are associated with exposure to lead, cadmium, mercury, and arsenic. Lead is predominantly stored in the skeleton [161]. This localization may be due to the capacity of CA to accumulate heavy elements [162]. Using synchrotron radiation-based micro-X-ray fluorescence analysis, Zoeger *et al.* [163, 164] have shown a highly selective accumulation of

Pb in the transition zone between calcified and non-calcified articular cartilage, the so-called “tidemark”. This tidemark transition zone is an active calcification front and is thus of great clinical importance. More recently, using XAS, Meirer *et al.* [93] have determined the state of Pb in this tidemark zone.

The same approach can be applied to calcified cartilage. For example, Bradley *et al.* [165] have explored the changes in mineralization associated with osteoarthritis development by X-ray diffraction and Ca and Sr  $K\alpha$  X-ray fluorescence microscopy. To achieve this, they analyzed lesions showing cartilage thinning and changes in the trabecular organization and density of the underlying bone. The complete set of data indicates that at the centre of the lesion the ratio of strontium to calcium was much lower than that in normal tissue, although the calcified cartilage still showed a higher ratio than the underlying bone. Moreover, in the superficially normal tissue around the lesion the calcified cartilage returned to a normal ratio much more rapidly than the underlying bone.

The presence of Zn in calcified cartilage has also been established, using a beamline able to collect XRD patterns and XAS spectra from the same sample (Figure 10) [166,167]. For this study, human carti-

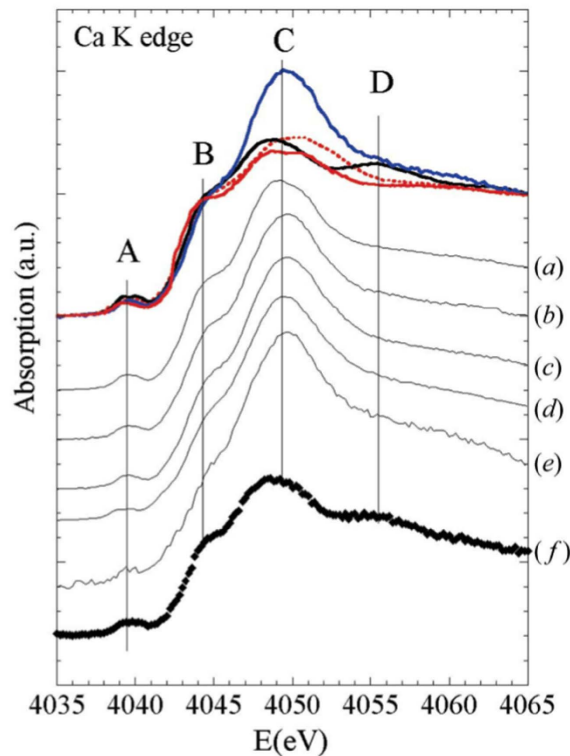


**Figure 9.** XANES spectra at Ca K-edge of human osteoarthritic cartilage, and reference synthetic calcium phosphate phases previously characterized by FTIR spectroscopy. Red solid line: synthetic nanocrystalline carbonated apatite (CA); red dotted line: amorphous carbonated calcium phosphate (ACCP); black solid line: m-CPPD; blue solid line: calcified tissue. (a) Patient 1, (b) Patient 3, (c) Patient 4, (d) Patient 5, (e) Patient 6 and (f) Patient 2 (from Ref. [92]).

lage (HC) and medial meniscus (MEM) samples were assigned a number.

Thus it was possible to characterize calcification by X-ray diffraction [168–175] while the environment of Zn was determined by XAS spectroscopy [94]. The complete set of data indicates that at least two Zn species were present: one may correspond to Zn metalloproteins (various Zn metalloproteins are known to inhibit biological calcification), and the other may be associated with a Zn “trap” in or on the surface of the calcification. Calcification in OA cartilage may significantly modify the spatial distribution of Zn, a fraction of which may be trapped in the calcification, altering the associated biological function of Zn metalloproteins.

## 5. Conclusion

The presence of apatite crystals has been reported to be associated with OA severity and cartilage degradation, whereas CPP is rather associated with chondrocyte senescence and aging [176]. While the contribution of the different types of calcium phosphate crystals to the clinical phenotype has been described, non-invasive imaging approaches to discriminate these calcifications are yet to be standardized.

In this article, we have described some of the physicochemical characteristics of various calcium phosphate phases identified in cartilage. Also, using a set of appropriate publications, we showed that it is possible to precisely describe not only the chemical composition and the spatial distribution of pathological calcifications in cartilage at the molecular and elemental level but also to detect trace elements



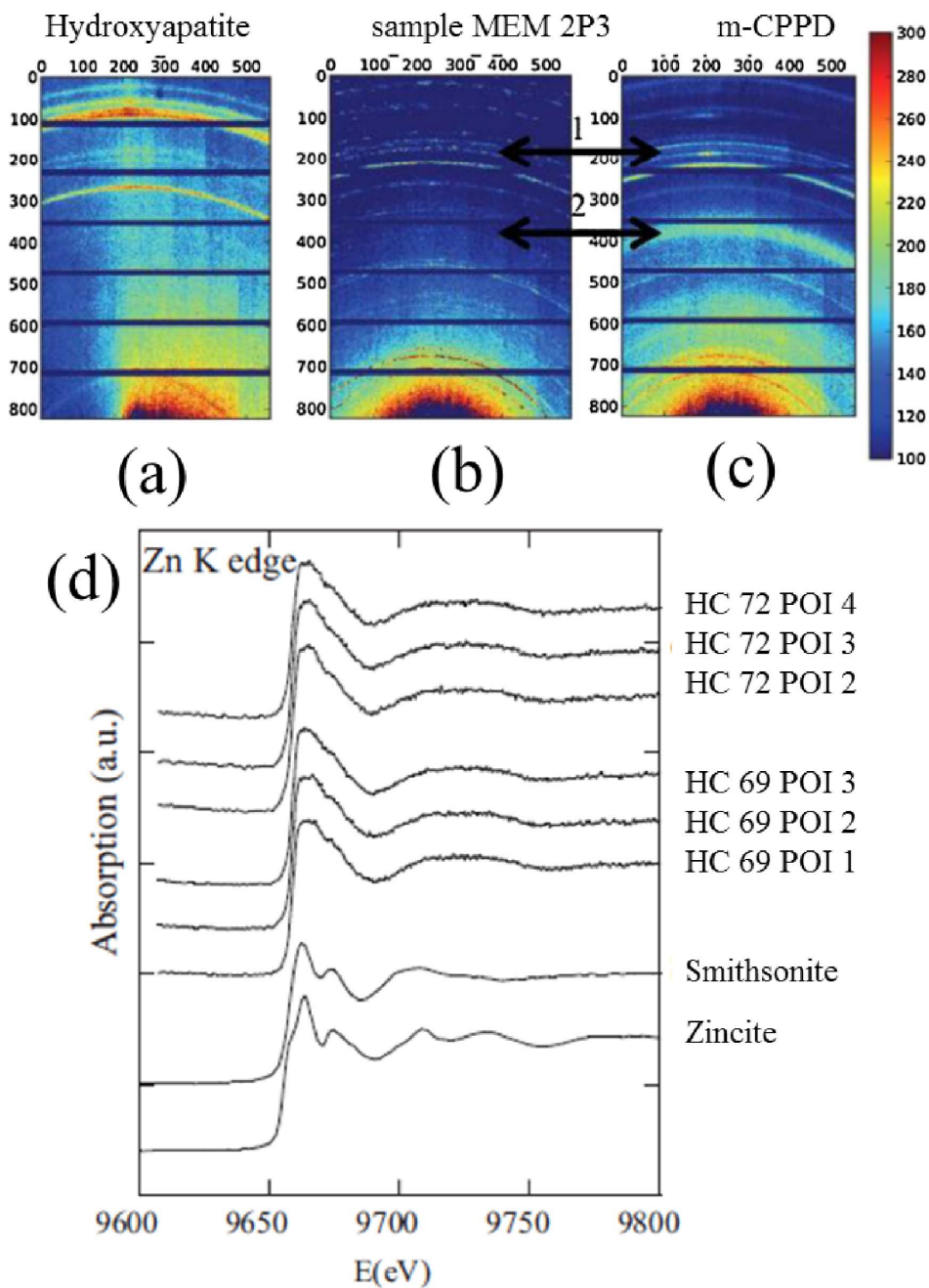


**Figure 10.** Micro-XRD analysis diagrams for the synthetic reference compounds and a biological specimen: (a) synthetic stoichiometric hydroxyapatite (HA), (b) biological sample MEM 2 P3, and (c) synthetic m-CPPD analyzed with the XPAD detector; (d)  $\mu$ XAS spectra recorded at the Zn K edge for biological samples (two calcified cartilage samples are considered namely HC69 and HC72 and for each of them, different points of interest (POI) have been considered in the study corresponding to Dessombz *et al.* [94]) and two reference compounds (smithsonite and zincite).



such as Zn which may be related to inflammatory processes.

Obviously, synchrotron radiation techniques offer further opportunities as shown by various excellent publications on cartilage as well as bone [177–181]. We hope that this contribution will reinforce collaboration between the medical and the physicochemical scientific communities.

## Conflicts of interest

Authors have no conflict of interest to declare.

## Acknowledgements

The authors thank the Centre National de la Recherche Scientifique (CalArthros project—“Longévité et Vieillessement 2010” CNRS interdisciplinary program) and the Agence Nationale de la Recherche (CAPYROSIS project—ANR-12-BS08-0022-01) for supporting part of this research work.

## References

- [1] Y. Zhang, J. M. Jordan, *Clin. Geriatr. Med.*, 2010, **26**, 355-369.
- [2] E. R. Vina, C. K. Kwok, *Curr. Opin. Rheumatol.*, 2018, **30**, 160-167.
- [3] *American Joint Replacement Registry (AJRR): 2020 Annual Report*, American Academy of Orthopaedic Surgeons (AAOS), Rosemont, IL, 2020.
- [4] L. Murphy, Ch. G. Helmick, *Am. J. Nurs.*, 2012, **112**, S13-S19.
- [5] D. J. Hunter, D. T. Felson, *Br. Med. J.*, 2006, **332**, 639-642.
- [6] R. F. Loeser, S. R. Goldring, C. R. Scanzello, M. B. Goldring, *Arthritis Rheum.*, 2012, **64**, 1697-1707.
- [7] H. Mitsuyama, R. M. Healey, R. A. Terkeltaub, R. D. Coutts, D. Amiel, *Osteoarth. Cart.*, 2007, **15**, 559-565.
- [8] B. Pazár, H. K. Ea, S. Narayan, L. Kolly, N. Bagnoud, V. Chobaz, T. Roger, F. Lioté, A. So, N. Busso, *J. Immunol.*, 2011, **186**, 2495-2502.
- [9] H.-K. Ea, V. Chobaz, C. Nguyen, S. Nasi, P. van Lent, M. Daudon, A. Dessombz, D. Bazin, G. McCarthy, B. Jolles-Haerberli, A. Ives, D. Van Linthoudt, A. So, F. Lioté, N. Busso, *PLoS One*, 2013, **8**, article no. e57352.
- [10] C.-L. Murphy, G. M. McCarthy, *EMJ Rheumatol.*, 2014, **1**, 96-102.
- [11] Y. Z. Liu, A. P. Jackson, S. D. Cosgrove, *Osteoarth. Cart.*, 2009, **17**, 1333-1340.
- [12] Ch. Nguyen, D. Bazin, M. Daudon, A. Chatron-Colliet, D. Hannouche, A. Bianchi, D. Côme, A. So, N. Busso, F. Lioté, H.-K. Ea, *Arthritis Res. Therapy*, 2013, **15**, article no. R103.
- [13] M. Fuerst, J. Bertrand, L. Lammers, R. Dreier, F. Echtermeyer, Y. Nitschke, F. Rutsch, F. K. W. Schäfer, O. Niggemeyer, J. Steinhagen, C. H. Lohmann, T. Pap, W. Rütther, *Arthritis Rheum.*, 2009, **60**, 2694-2703.
- [14] L. Campillo-Gimenez, F. Renaudin, M. Jalabert, P. Gras, M. Gosset, Ch. Rey, S. Sarda, C. Collet, M. Cohen-Solal, Ch. Combes, F. Lioté, H.-K. Ea, *Front Immunol.*, 2018, **9**, article no. 2248.
- [15] A. Yavorsky, A. Hernandez-Santana, G. McCarthy, G. McMahon, *The Analyst*, 2008, **133**, 302-318.
- [16] G. Devrimsel, M. S. Beyazal, A. K. Turkyilmaz, S. B. Sahin, *J. Phys. Therm. Sci.*, 2016, **28**, 2249-2252.
- [17] F. Eckstein, A. Guermazi, G. Gold, J. Duryea, M.-P. H. Le Graverand, W. Wirth, C. G. Miller, *Osteoarth. Cart.*, 2014, **22**, 1516-1532.
- [18] J. Sullivan, M. H. Pillinger, M. Toprover, *Curr. Rheumatol. Rep.*, 2021, **23**, article no. 77.
- [19] E. Cipolletta, G. Filippou, C. A. Scirè, A. Di Matteo, J. Di Battista, F. Salaffi, W. Grassi, E. Filippucci, *Osteoarth. Cart.*, 2021, **29**, 619-632.
- [20] T. Pascart, L. Norberciak, J. Legrand, F. Becce, J.-F. Budzik, *Osteoarth. Cart.*, 2019, **27**, 1309-1314.
- [21] T. Pascart, G. Falgayrac, L. Norberciak, C. Lalanne, J. Legrand, E. Houvenagel, H.-K. Ea, F. Becce, J. F. Budzik, *Therm. Adv. Musculoskelet. Dis.*, 2020, **24**, article no. 1759720X20936060.
- [22] L. K. Stamp, N. G. Anderson, F. Becce, M. Rajeswari, M. Polson, O. Guyen, A. Viry, Ch. Choi, T. E. Kirkbride, A. Y. Raja, *Arthritis Rheum.*, 2019, **71**, 1158-1162.
- [23] T. E. Kirkbride, A. Y. Raja, K. Müller, Ch. J. Bateman, F. Becce, N. G. Anderson, *AJR Am. J. Roentgenol.*, 2017, **209**, 1088-1092.
- [24] I. Bernabei, Y. Sayous, A. Y. Raja, M. R. Amma, A. Viry, S. Steinmetz, G. Falgayrac, R. van Heeswijk, P. Omoumi, T. Pascart, L. K. Stamp, S. Nasi, Th. Hügle, N. Busso, A. K. So, F. Becce, *Rheumatology (Oxford)*, 2021, **60**, 2483-2485, MARS Collaboration.
- [25] D. Bazin, M. Daudon, *Ann. Biol. Clin.*, 2015, **73**, 517-534.
- [26] D. Bazin, E. Boudierlique, M. Daudon, V. Frochot, J.-Ph. Haymann, E. Letavernier, F. Tielens, R. Weil, *C. R. Chim.*, 2022, **25**, no. S1, 37-60.
- [27] D. Bazin, M. Daudon, C. Combes, C. Rey, *Chem. Rev.*, 2012, **112**, 5092-5120.
- [28] D. Bazin, M. Daudon, *J. Phys. D: Appl. Phys.*, 2012, **45**, article no. 383001.
- [29] X. Cheng, D. G. Haggins, R. H. York, Y. N. Yeni, O. Akkus, *Appl. Spectrosc.*, 2009, **63**, 381-386.
- [30] J. N. Lalena, *Crystallogr. Rev.*, 2006, **12**, 125-180.
- [31] H. Kubbinga, *Z. Kristallogr.*, 2012, **227**, 1-26.
- [32] M. Van Meerssche, J. Feneau-Dupont, *Introduction à la Cristallographie et à la Chimie Structurale*, Vander, Louvain-Cesson, Belgium, 1973.
- [33] M. Vallet-Regi, M. J. Gonzalez-Calbet, *Prog. Solid. State. Chem.*, 2004, **32**, 1-31.
- [34] D. Bazin, C. Chappard, C. Combes, X. Carpentier, S. Rouzière, G. André, G. Matzen, M. Allix, D. Thiaudière, S. Reguer, P. Jungers, M. Daudon, *Osteoporos. Int.*, 2009, **20**, 1065-1075.
- [35] M. Banu, PhD Thesis, Polytechnic National Institute of Toulouse, 2005.
- [36] C. Rey, C. Combes, C. Drouet, A. Lebugle, H. Sfihi, A. Barroug, *Mater. Sci. Eng. Technol.*, 2007, **38**, 996-1002.
- [37] C. Drouet, C. Rey, *Nanostructured Biomaterials for Regener-*

- ative Medicine*, Woodhead Publishing Series in Biomaterials, Elsevier, Amsterdam, Netherlands, 2020, 223-254 pages.
- [38] D. Bazin, E. Letavernier, J. P. Haymann, V. Frochot, M. Daudon, *Ann. Biol. Clin.*, 2020, **78**, 349-362.
- [39] M. Daudon, V. Frochot, D. Bazin, P. Jungers, *C. R. Chim.*, 2016, **19**, 1514-1526.
- [40] J. R. Espinosa, C. Vega, Ch. Valeriani, D. Frenkel, E. Sanz, *Soft Matt.*, 2019, **15**, 9625-9631.
- [41] S. R. Khan, D. E. Rodriguez, L. B. Gower, M. Monga, *J. Urol.*, 2012, **187**, 1094-1100.
- [42] C. Gay, E. Letavernier, M.-Ch. Verpont, M. Walls, D. Bazin, M. Daudon, N. Nassif, O. Stephan, M. de Fruto, *ACS Nano.*, 2020, **14**, 1823-1836.
- [43] R. Coscas, M. Bensussan, M.-P. Jacob, L. Louedec, Z. Massy, J. Sadoine, M. Daudon, C. Chaussain, D. Bazin, J.-B. Michel, *Atherosclerosis*, 2017, **259**, 60-67.
- [44] H. Colboc, Ph. Moguelet, D. Bazin, P. Carvalho, A.-S. Dillies, G. Chaby, H. Maillard, D. Kottler, E. Goujon, Ch. Juras, M. Panaye, V. Frochot, E. Letavernier, M. Daudon, I. Lucas, R. Weil, Ph. Courville, J.-B. Monfort, F. Chasset, P. Senet, *JAMA Dermatol.*, 2019, **155**, 789-796.
- [45] H. Colboc, Ph. Moguelet, E. Letavernier, V. Frochot, J.-F. Bernaudin, R. Weil, S. Rouzière, P. Seneth, C. Bachmeyer, N. Laporte, I. Lucas, V. Descamps, R. Amodek, F. Brunet-Possentik, N. Kluger, L. Deschamps, A. Dubois, S. Reguer, A. Somogyi, K. Medjoubi, M. Refregiers, M. Daudon, D. Bazin, *C. R. Chim.*, 2022, **25**, no. S1, 445-476.
- [46] K. Nitiputri, Q. M. Ramasse, H. Autefage, C. M. McGilvery, S. Boonrungsiman, N. D. Evans, M. M. Stevens, A. E. Porter, *ACS Nano.*, 2016, **10**, 6826-6835.
- [47] H. C. Anderson, *J. Cell. Biol.*, 1969, **41**, 59-72.
- [48] S. Miyaki, M. K. Lotz, *Curr. Opin. Rheumatol.*, 2018, **30**, 129-135.
- [49] A. K. Rosenthal, *Curr. Opin. Rheumatol.*, 2016, **28**, 127-132.
- [50] J. C. Williams, J. E. Lingeman, M. Daudon, D. Bazin, *C. R. Chim.*, 2022, **25**, no. S1, 61-72.
- [51] C. Delecourt, M. Relier, S. Touraine, H. Bouhadoun, K. Engelke, J. D. Laredo, C. Chappard, *Osteoarth. Cart.*, 2016, **24**, 567-571.
- [52] M. U. Ghani, Z. Zhou, L. Ren, Y. Li, B. Zheng, K. Yang, H. Liu, *NIMA.*, 2016, **807**, 129-136.
- [53] M. Marenzana, Ch. K. Hagen, P. Das Neves Borges, M. Endrizzi, M. B. Szafraniec, T. L. Vincent, L. Rigon, F. Arfelli, R.-H. Menk, A. Olivo, *Phil. Trans. R. Soc. Lond. A*, 2014, **372**, article no. 20130127.
- [54] M. Daudon, M. F. Protat, R. J. Reveillaud, H. Jaeschke-Boyer, *Kidney Int.*, 1983, **23**, 842-850.
- [55] S. Tamosaityte, M. Pucetaite, A. Zelvys, S. Varvuolyte, V. Hendrixson, V. Sablinskas, *C. R. Chim.*, 2022, **25**, no. S1, 73-82.
- [56] I. T. Lucas, D. Bazin, M. Daudon, *C. R. Chim.*, 2022, **25**, no. S1, 83-103.
- [57] L. Estepa, M. Daudon, *Biospectroscopy*, 1997, **3**, 347-369.
- [58] M. Daudon, D. Bazin, *C. R. Chim.*, 2016, **19**, 1416-1423.
- [59] A. K. Rosenthal, E. Mattson, C. M. Gohr, C. J. Hirschmugl, *Osteoarth. Cart.*, 2008, **16**, 1395-1402.
- [60] Th. Debroise, E. Colombo, G. Belletti, J. Vekeman, Y. Su, R. Papoular, N. S. Hwang, D. Bazin, M. Daudon, P. Quaino, F. Tielens, *Cryst. Growth Des.*, 2020, **20**, 2553-2561.
- [61] A. Dessombz, D. Bazin, P. Dumas, C. Sandt, J. Sule-Suso, M. Daudon, *PLoS One*, 2011, **6**, article no. e28007.
- [62] N. Quy Dao, M. Daudon, *Infrared and Raman Spectra of Calculi*, Elsevier, Paris, 1997.
- [63] Z. Xu, Z. He, Y. Song, X. Fu, M. Rommel, X. Luo, A. Hartmaier, J. Zhang, F. Fang, *Micromachines (Basel)*, 2018, **9**, article no. 361.
- [64] R. S. Das, Y. K. Agrawal, *Vib. Spectrosc.*, 2011, **57**, 163-176.
- [65] A. Bonifacio, S. Cervo, V. Sergio, *Anal. Bioanal. Chem.*, 2015, **407**, 8265-8277.
- [66] J. M. Surmacki, B. J. Woodhams, A. Haslehurst, B. A. J. Ponder, S. E. Bohndiek, *Sci. Rep.*, 2018, **8**, article no. 12604.
- [67] G. S. Mandair, M. D. Morrisa, *Bonekey Rep.*, 2015, **4**, 1-8.
- [68] V. Frochot, V. Castiglione, I. T. Lucas, J.-P. Haymann, E. Letavernier, D. Bazin, G. B. Fogazzi, M. Daudon, *Clin. Chim. Acta*, 2021, **515**, 1-4.
- [69] H. Colboc, D. Bazin, P. Moguelet, S. Reguer, R. Amode, C. Jouanneau, I. Lucas, L. Deschamps, V. Descamps, N. Kluger, *J. Eur. Acad. Dermatol. Venereol.*, 2020, **34**, e313-e315.
- [70] P. Lasch, D. Naumann, *Biochim. Biophys. Acta*, 2006, **1758**, 814-829.
- [71] A. Dazzi, F. Glotin, R. Carminati, *J. Appl. Phys.*, 2010, **107**, article no. 124519.
- [72] A. Dazzi, C. B. Prater, *Chem. Rev.*, 2017, **17**, 5146-5173.
- [73] J. Mathurin, "Nanospectroscopie infrarouge avancée : développements instrumentaux et applications", PhD Thesis, Université Paris-Saclay, 2019.
- [74] E. Esteve, Y. Luque, J. Waeytens, D. Bazin, L. Mesnard, Ch. Jouanneau, P. Ronco, A. Dazzi, M. Daudon, A. Deniset-Besseau, *Anal. Chem.*, 2020, **92**, 7388-7392.
- [75] D. Bazin, M. Rabant, J. Mathurin, M. Petay, A. Deniset-Besseau, A. Dazzi, Y. Su, E. P. Hessou, F. Tielens, F. Borondics, M. Livrozet, E. Boudierlique, J.-Ph. Haymann, E. Letavernier, V. Frochot, M. Daudon, *C. R. Chim.*, 2022, **25**, no. S1, 489-502.
- [76] J. Mathurin, A. Deniset-Besseau, D. Bazin, E. Dartois, M. Wagner, A. Dazzi, *J. Appl. Phys.*, 2022, **131**, article no. 010901.
- [77] M. Kansiz, C. Prater, E. Dillon, M. Lo, J. Anderson, C. Marcott, A. Demissie, Y. Chen, G. Kunkel, *Microsc. Today*, 2020, **28**, 26-36.
- [78] C. Lima, H. Muhamadali, Y. Xu, M. Kansiz, R. Goodacre, *Anal. Chem.*, 2021, **93**, 3082-3088.
- [79] A. Spadea, J. Denbigh, M. J. Lawrence, M. Kansiz, P. Gardner, *Anal. Chem.*, 2021, **93**, 3938-3950.
- [80] P. Zhao, Y. Zhao, L. Cui, Y. Tian, Z. Zhang, Q. Zhu, W. Zhao, *Sci. Total Environ.*, 2021, **775**, article no. 145846.
- [81] D. Khanal, J. Zhang, W.-R. Ke, M. M. Banaszak Holl, H.-K. Chan, *Anal. Chem.*, 2020, **92**, 8323-8332.
- [82] D. Zhang, C. Li, C. Zhang, M. N. Slipchenko, G. Eakins, J.-X. Cheng, *Sci. Adv.*, 2016, **2**, article no. e1600521.
- [83] O. Klementieva, Ch. Sandt, I. Martinsson, M. Kansiz, G. K. Gouras, F. Borodics, *Adv. Sci.*, 2020, **7**, article no. 1903004.
- [84] D. Bazin, E. Boudierlique, E. Tang, M. Daudon, J.-Ph. Haymann, V. Frochot, E. Letavernier, E. Van de Perre, J. C. Williams Jr., J. E. Lingeman, F. Borondics, *C. R. Chim.*, 2022, **25**, no. S1, 105-131.
- [85] L. Rieppo, J. Töyräs, S. Saarakkala, *Appl. Spectrosc. Rev.*, 2017, **52**, 249-266.

- [86] N. P. Camacho, P. West, P. A. Torzilli, R. Mendelsohn, *Biopolymers*, 2001, **62**, 1-8.
- [87] K. Potter, L. H. Kidder, I. W. Levin, E. N. Lewis, R. G. Spencer, *Arthritis Rheum.*, 2001, **44**, 846-855.
- [88] R. G. Spencer, E. F. Calton, N. P. Camacho, *J. Biomed. Opt.*, 2006, **11**, article no. 064023.
- [89] D. E. Sayers, E. A. Stern, F. W. Lytle, *Phys. Rev. Lett.*, 1971, **27**, 1204-1207.
- [90] D. Bazin, D. Sayers, J. Rehr, *J. Phys. Chem. B*, 1997, **101**, 11040-11050.
- [91] D. Bazin, D. Sayers, J. J. Rehr, C. Mottet, *J. Phys. Chem.*, 1997, **101**, 5332-5336.
- [92] Ch. Nguyen, H. K. Ea, D. Thiaudiere, S. Reguer, D. Hannouche, M. Daudon, F. Lioté, D. Bazin, *J. Syn. Rad.*, 2011, **18**, 475-480.
- [93] F. Meirer, B. Pemmer, G. Pepponi, N. Zoeger, P. Wobruschek, S. Sprio, A. Tampieri, J. Goettlicher, R. Steininger, S. Mangold, P. Roschger, A. Berzlanovich, J. G. Hofstaettere, Ch. Strelt, *J. Synchrotron Rad.*, 2011, **18**, 238-244.
- [94] A. Dessombz, C. Nguyen, H.-K. Ea, S. Rouzière, E. Foy, D. Hannouche, S. Réguer, E.-E. Picca, D. Thiaudière, F. Lioté, M. Daudon, D. Bazin, *J. Trace Elem. Med. Biol.*, 2013, **27**, 326-333.
- [95] D. Brown, "Understanding the role of sulfur in cartilage development: How structural Proteoglycans are implicated in cartilage maturation", PhD Thesis, University of Saskatchewan, Saskatoon, 2017.
- [96] C. Bissardon, O. Proux, S. Bureau, E. Suess, L. H. E. Winkel, R. S. Conlan, L. W. Francis, I. M. Khan, L. Charlet, J. L. Hazemann, S. Bohic, *Analyst*, 2019, **144**, 3488-3493.
- [97] N. Mandel, G. Mandel, *Rheum. Dis. Clin. North Am.*, 1988, **14**, 321-340.
- [98] R. Legros, N. Balmain, G. Bonel, *Calcif. Tissue Int.*, 1987, **41**, 137-144.
- [99] G. M. Mccarthy, H. S. Cheung, *Curr. Rheumatol. Rep.*, 2009, **11**, 141-147.
- [100] D. J. McCarty, J. R. Lehr, P. B. Halverson, *Arthritis Rheum.*, 1983, **26**, 1220-1224.
- [101] D. McCarty, *Ann. Rheum. Dis.*, 1983, **42**, 243-253.
- [102] D. Bazin, R. J. Papoular, E. Elkaim, R. Weil, D. Thiaudière, C. Pisapia, B. Ménez, N. S. Hwang, F. Tielens, M. Livrozet, E. Boudierlique, J.-Ph. Haymann, E. Letavernier, L. Hennet, V. Frochot, M. Daudon, *C. R. Chim.*, 2022, **25**, no. S1, 343-354.
- [103] C. A. Scotchford, S. Y. Ali, *Ann. Rheum. Dis.*, 1995, **54**, 339-344.
- [104] D. Bazin, Ch. Jouanneau, S. Bertazzo, Ch. Sandt, A. Dessombz, M. Réfrégiers, P. Dumas, J. Frederick, J.-Ph. Haymann, E. Letavernier, P. Ronco, M. Daudon, *C. R. Chim.*, 2016, **19**, 1439-1454.
- [105] J. C. Elliott, *Structure and Chemistry of the Apatites and Other Calcium Orthophosphates*, Elsevier, Amsterdam, 1994.
- [106] T. J. White, D. Zhi Li, *Acta Crystallogr. B*, 2003, **59**, 1-16.
- [107] C. Rey, C. Combes, C. Drouet, H. Sfihi, A. Barroug, *Mater. Sci. Eng. C*, 2007, **27**, 198-205.
- [108] C. Rey, B. Collins, T. Goehl, I. R. Dickson, M. J. Glimcher, *Calcif. Tissue Int.*, 1989, **45**, 157-164.
- [109] R. Z. Legeros, *Monogr. Oral Sci.*, 1991, **15**, 1-201.
- [110] M. E. Fleet, X. Liu, *Biomaterials*, 2007, **28**, 916-926.
- [111] C. Combes, C. Rey, *Minerals*, 2016, **6**, article no. 34.
- [112] Y. Wu, M. J. Glimcher, C. Rey, J. L. Ackerman, *J. Mol. Biol.*, 1994, **244**, 423-435.
- [113] C. Rey, M. Shimizu, B. Collins, M. J. Glimcher, *Calcif. Tissue Int.*, 1990, **46**, 384-394.
- [114] S. Cazalbou, D. Eichert, X. Ranz, C. Drouet, C. Combes, M. F. Harmand, C. Rey, *J. Mater. Sci. Mater. Med.*, 2005, **16**, 405-409.
- [115] X. Cazalbou, C. Combes, D. Eichert, C. Rey, *J. Mater. Chem.*, 2004, **14**, 2148-2153.
- [116] D. Eichert, C. Drouet, H. Sfihi, C. Rey, C. Combes, "Nanocrystalline apatite-based biomaterials: synthesis, processing and characterization", in *Trends in Biomaterials Research* (P. J. Pannone, ed.), Nova Science Publishers, Inc., 2007, ISBN1-978-1-60021-361-8.
- [117] X. Carpentier, M. Daudon, O. Traxer, P. Jungers, A. Mazouyes, G. Matzen, E. Véron, D. Bazin, *Urology*, 2009, **73**, 968-975.
- [118] D. Bazin, G. André, R. Weil, G. Matzen, E. Véron, X. Carpentier, M. Daudon, *Urology*, 2012, **79**, 786-790.
- [119] C. Gervais, C. Bonhomme, D. Laurencin, *Solid State Nucl. Magn. Reson.*, 2020, **107**, article no. 101663.
- [120] S. Von Euw, W. Ajili, T.-H. C. Chan-Chang, A. Delices, G. Laurent, F. Babonneau, N. Nassif, T. Azaïs, *Acta Biomater.*, 2017, **59**, 351-360.
- [121] P. Pascaud, "Apatites nanocrystallines biomimétiques comme modèles de la réactivité osseuse : Etude des propriétés d'adsorption et de l'activité cellulaire d'un bisphosphonate, le tiludronate", PhD Thesis, Université de Toulouse, 2012.
- [122] M. Foster, S. Samman, *Nutrients*, 2012, **4**, article no. 676.
- [123] N. Z. Gammoh, L. Rink, *Nutrients*, 2017, **9**, article no. 624.
- [124] J. Olechnowicz, A. Tinkov, A. Skalny, J. Suliburska, *J. Phys. Sci.*, 2018, **68**, 19-31.
- [125] N. N. Kohn, R. E. Hughes, D. J. McCarty Jr., J. S. Faires, *Ann. Intern. Med.*, 1962, **56**, 738-745.
- [126] D. J. McCarty Jr., J. M. Hogan, R. A. Gatter, M. Grossman, *J. Bone Joint Surg. Am.*, 1966, **48**, 309-325.
- [127] T. Balić-Zunić, M. R. Christoffersen, J. Christoffersen, *Acta Crystallogr. B*, 2000, **56**, 953-958.
- [128] C. I. R. De Oliveira, L. F. C. de Oliveira, F. A. Dias Filho, Y. Messaddeq, S. J. L. Ribeiro, *Spectrochim. Acta. A*, 2005, **61**, 2023-2028.
- [129] C. Roiland, F. Fayon, P. Simon, D. Massiot, *J. Non. Cryst. Solids*, 2011, **357**, 1636-1646.
- [130] P. Gras, "Physico-chemical and structural study of hydrated calcium pyrophosphates: application to microcalcifications associated with arthritis", PhD Thesis, Toulouse University, 2014.
- [131] P. Gras, C. Rey, O. Marsan, S. Sarda, C. Combes, *Eur. J. Inorg. Chem.*, 2013, **34**, 5886-5895.
- [132] P. Gras, N. Ratel-Ramond, S. Teychené, C. Rey, E. Elkaim, B. Biscans, S. Sarda, C. Combes, *Acta Crystallogr. C*, 2014, **70**, 862-866.
- [133] E. H. Brown, J. R. Lehr, J. P. Smith, A. W. Frazier, *J. Agric. Food. Chem.*, 1963, **11**, 214-222.
- [134] C. Slater, D. Laurencin, V. Burnell, M. E. Smith, L. M. Grover, J. A. Hriljac, A. J. Wright, *J. Mater. Chem.*, 2011, **21**, 18783-18791.
- [135] P. Gras, C. Rey, G. André, C. Charvillat, S. Sarda, C. Combes, *Acta Crystallogr. B*, 2016, **72**, 96-101.

- [136] R. B. Stockbridge, R. Wolfende, *J. Biol. Chem.*, 2011, **286**, 18538-18546.
- [137] O. Proux, E. Lahera, W. Del Net, I. Kieffer, M. Rovezzi, D. Testemale, M. Irar, S. Thomas, A. Aguilar-Tapia, E. F. Bazarkina, A. Prat, M. Tella, M. Auffan, J. Rose, J. L. Hazemann, *J. Environ Qual.*, 2017, **46**, 1146-1157.
- [138] N. S. Mandel, *Acta Crystallogr. B—Struct. Sci.*, 1975, **31**, 1730-1734.
- [139] L. Campillo-Gimenez, F. Renaudin, M. Jalabert, P. Gras, M. Gosset, C. Rey, S. Sarda, C. Collet, M. Cohen-Solal, C. Combes, F. Lioté, H.-K. Ea, *Front Immunol.*, 2018, **9**, article no. 2248.
- [140] M. Roch-Arveiller, R. Legros, B. Chanaud, O. Muntaner, S. Strzalko, A. Thuret, D. A. Willoughby, J. P. Giroud, *Biomed. Pharmacother.*, 1990, **44**, 467-474.
- [141] F. Porcaro, S. Roudeau, A. Carmona, R. Ortega, *Trends Anal. Chem.*, 2018, **104**, 22-41.
- [142] X. Carpentier, D. Bazin, P. Jungers, S. Reguer, D. Thiaudière, M. Daudon, *J. Synchrotron Rad.*, 2010, **17**, 374-379.
- [143] R. F. Weska, C. G. Aimoli, G. M. Nogueira, A. A. Leirner, M. J. S. Maizato, O. Z. Higa, B. Polakievicz, R. N. M. Pitombo, M. M. Beppu, *Artif. Organs*, 2010, **34**, 311-318.
- [144] L. Pascolo, A. Gianoncelli, C. Rizzardi, V. Tisato, M. Salomé, C. Calligaro, F. Salvi, D. Paterson, P. Zamboni, *Sci. Rep.*, 2014, **4**, article no. 6540.
- [145] V. Martin-Diaconescu, M. Gennari, B. Gerey, E. Tsui, J. Kanady, R. Tran, J. Pécaut, D. Maganas, V. Krewald, E. Gouré, C. Duboc, J. Yano, Th. Agapie, M.-N. Collomb, S. DeBeer, *Inorg. Chem.*, 2015, **54**, 1283-1292.
- [146] D. Bazin, X. Carpentier, O. Traxer, D. Thiaudière, A. Somyi, S. Reguer, G. Waychunas, P. Jungers, M. Daudon, *J. Synchrotron Rad.*, 2008, **15**, 506-509.
- [147] D. Bazin, X. Carpentier, I. Brocheriou, P. Dorfmüller, S. Aubert, Ch. Chappard, D. Thiaudière, S. Reguer, G. Waychunas, P. Jungers, M. Daudon, *Biochimie*, 2009, **91**, 1294-1300.
- [148] D. Bazin, A. Dessombz, Ch. Nguyen, H. K. Ea, F. Lioté, J. Rehr, Ch. Chappard, S. Rouzière, D. Thiaudière, S. Reguer, M. Daudon, *J. Synchrotron Rad.*, 2014, **21**, 136-142.
- [149] D. Bazin, M. Daudon, Ch. Chappard, J. J. Rehr, D. Thiaudière, S. Reguer, *J. Synchrotron Rad.*, 2011, **18**, 912-918.
- [150] E. Esteve, D. Bazin, Ch. Jouanneau, S. Rouzière, A. Bataille, A. Kellum, K. Provost, Ch. Mocuta, S. Reguer, D. Thiaudière, K. Jorissen, J. J. Rehr, A. Hertig, E. Rondeau, E. Letavernier, M. Daudon, P. Ronco, *C. R. Chim.*, 2016, **19**, 1580-1585.
- [151] E. Esteve, D. Bazin, Ch. Jouanneau, S. Rouzière, A. Bataille, A. Kellum, K. Provost, Ch. Mocuta, S. Reguer, D. Thiaudière, K. Jorissen, J. J. Rehr, A. Hertig, E. Rondeau, E. Letavernier, M. Daudon, P. Ronco, *C. R. Chim.*, 2016, **19**, 1586-1589.
- [152] E. Esteve, S. Reguer, C. Boissière, C. Chanéac, G. Lugo, Ch. Jouanneau, C. Mocuta, D. Thiaudière, N. Leclercq, B. Leyh, J.-F. Greisch, J. Berthault, M. Daudon, P. Ronco, D. Bazin, *J. Synchrotron Rad.*, 2017, **24**, 991-999.
- [153] D. Bazin, *C. R. Chim.*, 2022, **25**, no. S3, Forthcoming.
- [154] J. Moonen, J. Slot, L. Lefferts, D. Bazin, H. Dexpert, *Physica B*, 1995, **208-209**, 689-690.
- [155] D. Bazin, J. Rehr, *J. Phys. Chem. B*, 2003, **107**, 12398-12402.
- [156] D. Bazin, J. Rehr, *J. Phys. Chem. C*, 2011, **115**, 23233-23236.
- [157] D. Eichert, M. Salome, M. Banu, J. Susini, C. Rey, *Spectrochim. Acta B*, 2005, **60**, 850-858.
- [158] K. Asokan, J. C. Jan, J. W. Chiou, W. F. Pong, P. K. Tseng, I. N. Lin, *J. Synchrotron Radiat.*, 2001, **8**, 839-841.
- [159] J. Chaboy, S. Quartieri, *Phys. Rev. B*, 1995, **52**, 6349-6357.
- [160] L. Jarup, *Br. Med. Bull.*, 2003, **68**, 167-182.
- [161] L. E. Wittmers, J. Wallgren, A. Alich, A. C. Aufderheide, G. Rapp, *Arch. Environ. Health*, 1988, **43**, 381-391.
- [162] J. Boisson, A. Ruttens, M. Mench, J. Vangronsveld, *Environ. Pollut.*, 1999, **104**, 225-233.
- [163] N. Zoeger, P. Roschger, J. Hofstaetter, C. Jokubonis, G. Pèponi, G. Falkenberg, P. Fratzl, A. Berzlanovich, W. Osterode, C. Strelt, P. Wobraschek, *Osteoarth. Cart.*, 2006, **14**, 906-913.
- [164] N. Zoeger, C. Strelt, P. Wobraschek, C. Jokubonis, G. Pèponi, P. Roschger, J. Hofstaetter, A. Berzlanovich, D. Wegrynek, E. Chinea-Cano, A. Markowicz, R. Simon, G. Falkenberg, *X-ray Spectrom.*, 2008, **37**, 3-11.
- [165] D. A. Bradley, P. Muthuvelu, R. E. Ellis, E. M. Green, D. Attenburrow, R. Barrett, K. Arkill, D. B. Colridge, C. P. Winlove, *NIM B*, 2007, **263**, 1-6.
- [166] S. Reguer, C. Mocuta, D. Thiaudière, M. Daudon, D. Bazin, *C. R. Chim.*, 2016, **19**, 1424-1431.
- [167] D. Bazin, S. Reguer, D. Vantelon, J.-Ph. Haymann, E. Letavernier, V. Frochot, M. Daudon, E. Esteve, H. Colboc, *C. R. Chim.*, 2022, **25**, no. S1, 189-208.
- [168] A. Guinier, *Théorie et Technique de la Radiocristallographie*, Dunod, Paris, 1964.
- [169] A. Le Bail, *Mater. Sci. Forum*, 2001, **378-381**, 65-70.
- [170] D. Bazin, L. Guzzi, J. Lynch, *Appl. Catal. A*, 2002, **226**, 87-113.
- [171] A. Le Bail, D. Bazin, M. Daudon, A. Brochot, V. Robbez-Masson, V. Maisonneuve, *Acta Crystallogr. B*, 2009, **65**, 350-354.
- [172] M. Daudon, D. Bazin, K. Adil, A. Le Bail, *Acta Crystallogr. E*, 2011, **67**, article no. o1458.
- [173] A. Le Bail, M. Daudon, D. Bazin, *Acta Crystallogr. C*, 2013, **69**, 734-737.
- [174] S. Rouzière, D. Bazin, M. Daudon, *C. R. Chim.*, 2016, **19**, 1404-1415.
- [175] D. Bazin, V. Frochot, J.-Ph. Haymann, E. Letavernier, M. Daudon, *C. R. Chim.*, 2022, **25**, no. S1, 133-147.
- [176] S. Stücker, M. Bollmann, Ch. Garbers, J. Bertrand, *Best Pract. Res. Clin. Rheumatol.*, 2021, **35**, article no. 101722.
- [177] R. Cancedda, A. Cedola, A. Giuliani, V. Komlev, S. Lagomarsino, M. Mastrogiacomo, F. Peyrin, F. Rustichelli, *Biomaterials*, 2007, **28**, 2505-2524.
- [178] A. D. Olubamiji, Z. Izadifar, D. Xiongbiao Chen, *Tissue Eng. Part B Rev.*, 2014, **20**, 503-522.
- [179] Z. Izadifar, L. D. Chapman, X. Chen, *Tissue Eng. Part C Meth.*, 2014, **20**, 140-148.
- [180] A. Horng, E. Brun, A. Mittone, S. Gasilov, L. Weber, T. Geith, S. Adam-Neumair, S. D. Auweter, A. Bravin, M. F. Reiser, P. Coan, *Invest. Radiol.*, 2014, **49**, 627-634.
- [181] A. Horng, J. Stroebel, T. Geith, S. Milz, A. Pacureanu, Y. Yang, P. Cloetens, G. Lovric, A. Mittone, A. Bravin, P. Coan, *J. Biomed. Sci.*, 2021, **28**, article no. 42.